193-nm lithography (Review Paper)

Rothschild, Mordechai, Forte, Anthony, Horn, Mark, Kunz, Roderick, Palmateer, Susan, et al.

Mordechai Rothschild, Anthony R. Forte, Mark W. Horn, Roderick R. Kunz, Susan C. Palmateer, Jan H. C. Sedlacek, "193-nm lithography (Review Paper)," Proc. SPIE 2703, Lasers as Tools for Manufacturing of Durable Goods and Microelectronics, (8 April 1996); doi: 10.1117/12.237751

SPIE.

Event: Photonics West '96, 1996, San Jose, CA, United States

Review Paper

193-nm Lithography

M. Rothschild, A. R. Forte, M. W. Horn, R. R. Kunz, S. C. Palmateer, and

J. H. C. Sedlacek

Lincoln Laboratory, Massachusetts Institute of Technology

Lexington, Massachusetts 02173-9108

ABSTRACT

The trend in microelectronics toward printing features 0.25 μm and below has motivated the development of lithography at the 193-nm wavelength of argon fluoride excimer lasers. This technology is in its early stages, but a picture is emerging of its strengths and limitations. The change in wavelength from 248 to 193 nm will require parallel progress in projection systems, optical materials, and photoresist chemistries and processes. This paper reviews the current status of these various topics, as they have been engineered under a multi-year program at MIT Lincoln Laboratory.

Keywords: excimer, lithography, photo resists, optical materials, silylation, projection optics

I. INTRODUCTION

The relentless drive in the integrated circuit industry toward greater packing density and higher speeds has served as the impetus for optical lithography to reduce printed image sizes from 2 μm twenty years ago to sub-0.5 μm today. This remarkable progress has been made possible by improved lens quality, increases in numerical aperture, improved resist processes, and the use of increasingly shorter exposure wavelengths. Today's photolithography uses wavelengths of 365 or 248 nm for imaging the smallest possible feature sizes, thus employing aggressively low lithographic k_1 factors of 0.5 to 0.6. But as image dimension requirements drop below 0.25 μm in the next few years, it will be necessary to consider even shorter exposure wavelengths. An obvious candidate for extension to shorter wavelengths is the 193-nm laser line produced by the argon fluoride (ArF) excimer laser.

The change to 193 nm poses challenges and opens up new possibilities, as new photoinduced processes take place at this shorter wavelength. Specifically, nominally transparent optical materials have residual absorption and also undergo laser induced changes, and fewer organic polymers are transparent enough to serve as single layer resists. On the other hand, efficient photoinduced crosslinking or oxidation of silicon containing polymers may enable new near-surface resist processes.

In this paper we review the progress that has been made at MIT Lincoln Laboratory towards a production-worthy 193-nm technology at sub-0.25-μm resolution.[1] The Lincoln Laboratory program has addressed in parallel both the construction of a full field prototype exposure system (including the evaluation of optical materials and coatings) and the development of photoresist processes (single layer, antireflective layer, top surface imaging, bilayers, and all-dry resists).

II. PROJECTION SYSTEM

A full field prototype 193-nm step-and-scan exposure system was built by SVGL, and it was installed in Lincoln Laboratory's cleanroom at the end of 1993. This system is the world's first — and presently only — large field 193-nm prototype exposure tool. It has a 193-nm 0.50-numerical aperture (NA) lithographic lens with 4X demagnification, mounted on a commercial SVGL Micrascan II body. The scanned field is 22 × 32.5 mm.

The Micrascan uses a catadioptric lens design, incorporating both reflective and refractive optical elements. The chromatic aberration of this design is low enough to accommodate the natural 0.5-nm excimer laser bandwidth.[2] The ability of the catadioptric lens to use the natural bandwidth of the ArF laser considerably eases the demands on the laser design.

The laser in the 193 Micrascan was built by Cymer Laser. It is able to produce its designed 6-W average power (linearly polarized) at 350 Hz with new optical elements. As the laser ages, the power level characteristically drops, owing to increased

0-8194-2077-8/96/$6.00

levels of damage in bulk optical materials and coatings within the laser. Replacement of damaged optical elements essentially restores the laser to its original power level. Typical lifetimes of optical components within the laser range from several weeks to several months, with large variations among materials from different sources.

III. OPTICAL MATERIALS

In parallel with the construction of the 193-nm Micrascan we have been studying the performance of optical materials at 193 nm. Few optical materials are transparent enough at 193 nm to enable the fabrication of a high-quality all-refractive or catadioptric system as required for a lithographic lens. High-purity synthetic fused silica and crystalline calcium fluoride are probably the only practical choices,[3] with fused silica having the edge for reasons of cost and existing processing infrastructure. For purposes of insertion into 193-nm lithography, the ideal optical material should be fully transparent, and should remain unchanged after several billions of pulses. In practice, fused silica has an absorption coefficient of 0.005 to 0.10 cm^{-1} with large variations from grade to grade and even from sample to sample. Since the temperature coefficient of the index of refraction of fused silica at 193 nm is $\sim 2.0 \times 10^{-5}$ $°C^{-1}$, the magnitude of allowable absorption coefficient will be determined by system considerations, including laser power and the specific design of the projection optics. A value of 0.10 cm^{-1} is clearly unacceptable, but the range 0.001 to 0.01 cm^{-1} requires careful analysis with respect to each system design.

Beyond the amount of initial absorption and scattering, the optical material should be resistant to radiation induced changes ("damage") over the practical lifetime of a projection system. The principal modes of laser induced damage in fused silica are color center formation and optical compaction.[4] The color centers are E' centers which are an unpaired electron on a silicon atom, accompanied by oxygen vacancy. Formation of E' color centers leads to absorption at ~215 nm, with increased optical absorption also at 193 nm. Compaction manifests itself as reduced thickness accompanied by an increased index of refraction.[4,5] The net result is a change in the optical path, which in a lithographic lens would cause wavefront aberrations and loss of image quality. The two types of damage seem to depend on different properties of the fused silica; a sample with good resistance to color center formation does not necessarily have good resistance to compaction. Typical samples seem to be more sensitive to compaction than to color center formation, and currently this sets the limit on allowable power densities within the lithographic lens.

Calcium fluoride (CaF_2) does not suffer from compaction, due to the crystalline nature of the material. It is susceptible to color center formation, but this susceptibility is apparently due only to defects and impurities in the material. Current high purity CaF_2 is significantly better than that available a decade ago. In fact, it is comparable to or better than fused silica in its resistance to damage.[6] The main technical barriers against extensive use of calcium fluoride as a 193-nm lens material are residual stress birefringence, and lack of experience with its grinding and polishing characteristics.

It should be noted that the results discussed above have been obtained from experiments performed off-line. To date, there is no evidence that the Micrascan optics (section II) has suffered the kind of bulk damage seen on samples at higher fluences.

The properties of bulk optical materials are but one item in the list of optics-related topics that need to be addressed at 193 nm. Others include the behavior of dielectric coatings,[3] pellicles,[7] and photoinduced organic deposits on surfaces. These are also the subject of ongoing studies at Lincoln Laboratory.

IV. SINGLE LAYER RESISTS

The most difficult challenge in bringing 193-nm lithography to full manufacturing use is the development of a robust photoresist process. The resins which are typically used for i-line and 248-nm photoresists, e.g., novolac, poly(hydroxystyrene), have absorption depths of 30 to 50 nm at 193 nm, and therefore are far too opaque to be used in single layer resists at that wavelength.

Until recently, the only single layer resist that has been demonstrated to work at 193 nm has been poly(methyl methacrylate), but its sensitivity is very low, with doses greater than 1 J/cm^2 required. More advanced methacrylate-based systems which operate via acid-catalyzed conversion of *t*-butyl methacrylate (tBMA) into methacrylic acid (MAA) have been developed for

laser direct-write applications at visible-laser wavelengths.[8] Since methacrylates are semitransparent at 193 nm, these resists are easily adapted for use at this wavelength. Several versions of such resists have indeed been developed under a collaboration between MIT Lincoln Laboratory and IBM-Almaden Research Center.[9,10]

These systems contain resins synthesized by free-radical solution terpolymerization of tBMA (fraction x), MMA (fraction y), and MAA (fraction z), and meet the transparency and thermal stability requirements for single layer resist applications. A typical composition has $x/y/z \approx 0.4/0.4/0.2$, and the glass transition temperature (T_g) is in the range 140 to 160 °C. The absorption coefficient of these base resins at 193 nm is around 0.08 μm^{-1}.

The solubility of these terpolymers can be controlled by variations in MAA content. For example, when the MAA concentration is ~20 mole percent, the exposed films are aqueous-base soluble only after exposure, whereas at MAA fractions approaching 30 mole percent, the unexposed resin itself becomes aqueous-base soluble.

Since the lithographic process requires acid-catalyzed chemical amplification, the resist formulation must contain a photoacid generator (PAG) in addition to the base resin. Depending on the type of PAG used, the amount that can be added to the resist may be limited by its absorbance at 193 nm. Figure 1 shows a contrast curve for a formulation containing 1 wt% of bis(t-butlyphenyl) iodonium triflate. The contrast γ as determined from Figure 1 is 3.5. It is clear that even with aromatic-containing PAGs, a large window in formulation exists that will allow optimal photospeed, good contrast, and high transparency. The performance at 248 nm of such a two-component resist, including resolution, exposure latitude and depth of focus, is similar to that of APEX-E, a standard commercially available 248-nm resist. Further improvements in increasing sensitivity, contrast, and dissolution rate ratio have been obtained by adding a third component to the resist, namely, a dissolution inhibitor. Recent versions of such systems have been tested at 248 nm and have printed features at lithographic k_1 factors of ~0.5.[10]

The main drawback of these photoresists is their low etch resistance in subsequent plasma processing steps, especially in the chlorine-based chemistries required for metal etching. Increased etching resistance can be obtained by incorporation of high-carbon-content polymers. These cannot be aromatics because of limitations of transparency. The alternative is copolymerization with polymers containing pendant alicyclics, such as adamantyl methacrylates.[11] Resultant tetrapolymers have been synthesized and have been shown to have significantly lower etch rates, 1.4× that of novolac, compared to 2.2× that of novolac for the terpolymers.

The use of single layer resists at 193 nm requires also the development of suitable antireflective layers (ARL). Such layers are needed, just as at 248 nm, to minimize swing curve fluctuations caused by reflections from the substrate, especially when it is non planar. To be effective the ARL must have certain optical and chemical characteristics.[12] For a bottom ARL (applied between the substrate and the resist), the index would be closely matched to that of the resist ($n_{193} = 1.685$ for 193-nm resist) with κ_{193} around 0.30.

The design approach for the 193-nm bottom ARL involves use of a transparent, aliphatic polymer matrix in a phase-compatible blend with an aromatic polymer dye. There were several considerations involved in determination of this design approach, the most important of which was that monomeric dyes were to be avoided to minimize any possible interdiffusion between the ARL and the chemically amplified resist, which may be prone to poisoning. To permit design simplicity, we chose polymer blends between novolacs and methacrylates. These blends have been reported as highly phase compatible and have successfully been used as i-line, deep-UV, and X-ray resists.[13] To prevent dissolution of the ARL during the spin casting of the photoresist, the methacrylate component contains an epoxide crosslinker. The typical composition contains a copolymer between MMA and dicyclopentadienyloxy methacrylate (DCPOMA) in a blend with novolac. The epoxy group induces crosslinking when heated in the presence of phenolics; the exact structure and concentration of this group dictate the amount of annealing necessary for complete insolubilization. The bake conditions required to render a poly(MMA-*co*-DCPOMA)/novolac blend insoluble in propylene glycol monomethylether acetate are 180°C for 10 minutes.

Imaging experiments over topography with and without such an ARL were performed on a home-built, small-field 0.22-NA stepper[14] and the results are shown in Fig. 2. The ARL was roughly 200 nm thick, and the underlying topography consisted of 500-nm-high poly-Si steps. The improved linewidth uniformity seen in Fig. 2 clearly indicates that our optimized ARL significantly improves resist performance.

V. TOP SURFACE IMAGING

Top surface imaged (TSI) resists have been developed at longer wavelengths as an alternative to bulk imaged resists.[15] Their main potential advantages are a larger depth of focus, especially for sub-0.25-μm lithography, where the thickness of single layer resists becomes comparable to the theoretical optical depth of focus, and the elimination of the need for ARLs. TSI processes operate via area-selective in-diffusion of a silyl amine into a phenolic polymer to form a silyl ether. Once the silicon has been selectively incorporated, the latent image is developed in an anisotropic oxygen plasma etch. At 193 nm, the simplest TSI resist scheme is a positive-tone process, based on photocrosslinking of the single component poly(vinylphenol) (PVP), followed by selective silylation of the unexposed areas and plasma etching.[16]

The overall lithographic performance of the silylation process depends on both the silylation step (i.e., the silylation mask shape) and the dry development step (i.e., selectivity, vertical/lateral etch rates and amount of overetch). Figure 3 demonstrates the excellent linearity obtained with the 0.5-NA 193-nm Micrascan and the TSI process outlined above. For a wafer temperature in the helicon etcher of -70°C, linearity is maintained down to 0.20 μm for both a 25 and 100% overetch. For an etch temperature of 30°C, linearity is maintained down to 0.20 μm for a 25% overetch, but only to 0.30 μm for a 100% overetch. This is due to an increased isotropic etching component at 30°C. The nominal best dose for a 100% overetch is 20% lower than for a 25% overetch in order to enable more silylation which compensates for the longer etch. The grating-to-isolated-line bias for a 60-s silylation time decreases from 30 nm for the 25% overetch, to 5 nm for the 100% overetch. For a 30-s silylation time the grating-to-isolated-line bias is reduced to 5 nm for a 25% overetch. Dense feature linearity was extended down to 0.175 μm by reducing the silylation time from 60 to 30 s.

In addition to linearity, lithographic performance is also judged by the extent of the exposure and defocus process latitudes. Figure 5 is a plot of total exposure latitude vs feature size (gratings) for a 30- and 60-s silylation time and a 25% overetch. For the smaller features the exposure latitude increases for the thinner silylated thickness. Note that even for features as small as 0.175 μm, exposure latitudes of at least 20% are obtained.

Figure 4 is a graphic representation of the exposure-dose matrix for 0.25-, 0.20- and 0.175-μm gratings for a 30-s silylation time and a 25% overetch. At best dose the depth of focus is 1.6, 1.0, and 1.0 μm, respectively. However, this maximum depth of focus is obtained at higher doses as the feature size decreases. Such behavior is in qualitative agreement with aerial image simulations and corresponding exposure-defocus plots. The simulation predicts an 8.5% increase in best dose when the grating lines are reduced from 0.25 to 0.20 μm. This result is in close agreement with the 10% dose increase measured experimentally. The experimentally measured depth of focus values are less than those predicted theoretically. This is to be expected, since the simulation is only of the aerial image and does not take into account the silylation and etch steps. It should be noted that the data tabulated above are based on printed features which have near vertical sidewalls. Figure 5 shows representative SEMs of 0.20-, 0.175-, and 0.15-μm resist features obtained as described above.

VI. CONCLUSIONS

Fundamental optics principles have motivated the trend in photolithography towards shorter wavelengths. One of the main alternatives for printing 0.18-μm devices, whose mass production is expected to start around the year 2001, is lithography at the 193-nm wavelength of ArF excimer lasers. The transition from 248 to 193 nm is viewed as largely evolutionary, following the trend from 436 to 365 to 248 nm. Nevertheless, new infrastructures need to be developed, mainly in the areas of optical materials and photoresists. Under the MIT Lincoln Laboratory program, a full field 193-nm prototype step-and-scan system has been built, and is currently undergoing tests and modifications of its subsystems. Bulk optical materials and coatings are continuously being tested for absorption and resistance to laser induced damage. First-generation single layer resist systems (including antireflective layers) and TSI processes have been developed. Initial experimental results indicate that key requirements of such resists, such as 0.18-μm resolution and 1-μm depth of focus, can indeed be met. Other resist schemes have also been demonstrated, although they are technically less mature than TSI, and therefore have not been detailed in this paper. These include bilayer resists with polysilyne imaging layers,[17] and plasma-deposited, plasma-developed counterparts of bilayers and of TSI ("all-dry resists").[18,19] Significant additional work is, however, required in order to transform the current proof-of-concept demonstrations into a robust manufacturing technology. Critical associated

technologies need to be developed and tested as well. These include overlay, metrology, and mask writing — all at the dimensions dictated by the insertion point of 0.18-μm critical dimension. Some of these technologies, such as overlay, are not specific to the 193-nm actinic wavelength, while others, such as materials for attenuating phase shifting masks, are. They all have to be brought to a significant level of maturity at an accelerated pace, so as to enable insertion into pilot lines within the next three years.

ACKNOWLEDGMENT

We thank D. Downs, L. Eriksen, and B. Maxwell for their technical assistance. The work presented in Section 4 was performed under a collaboration with IBM-Almaden Research Center, mainly with R. D. Allen, R. A. DiPietro, D. C. Hofer, and G. M. Wallraff. This work was sponsored by the Advanced Research Projects Agency's Advanced Lithography Program. Opinions, interpretations, conclusions, and recommendations are those of the authors and are not necessarily endorsed by the United States Air Force.

REFERENCES

1. For an earlier review, see: M. Rothschild, R. B. Goodman, M. A. Hartney, M. W. Horn, R. R. Kunz, J. H. C. Sedlacek, and D. C. Shaver, *J. Vac. Sci. Technol. B* **10**, 2989 (1992).

2. R. Sandstrom, *SPIE Proc.* **1463**, 610 (1991).

3. M. Rothschild, *Opt. and Photon. News* **4**, (5), 8 (1993).

4. M. Rothschild and J. H. C. Sedlacek, *SPIE Proc.* **1848**, 537 (1992).

5. R. Schenker, P. Schermerhorn, and W. G. Oldham, *J. Vac. Sci. Technol. B* **12**, 3275 (1994).

6. J. H. C. Sedlacek and M. Rothschild, *SPIE Proc.* **1835**, 80 (1992).

7. M. Rothschild and J. H. C. Sedlacek, *SPIE Proc.* **1674**, 618 (1992).

8. R. D. Allen, G. M. Wallraff, W. D. Hinsberg, and L. L. Simpson, *J. Vac. Sci. Technol. B* **9**, 3357 (1991).

9. R. R. Kunz, R. D. Allen, W. D. Hinsberg, and G. M. Wallraff, *SPIE Proc.* **1925**, 167 (1993).

10. R. D. Allen, G. M. Wallraff, R. A. DiPietro, D. C. Hofer, and R. R. Kunz, in *Proc. Am. Chem. Soc. Natl. Symp. 1995* (in press).

11. Y. Kaimoto, K. Nozaki, S. Takechi, and N. Abe, *SPIE Proc.* **1672**, 66 (1992).

12. R. R. Kunz and R. D. Allen, *SPIE Proc.* **2195**, 447 (1994).

13. R. D. Allen, Q. P. Ly, G. M. Wallraff, C. E. Larson, W. D. Hinsberg, W. E. Conley, and K. P. Muller, *SPIE Proc.* **1925**, 246 (1993).

14. D. C. Shaver, D. M. Craig, C. A. Marchi, M. A. Hartney, and F. Goodall, *SPIE Proc.* **1676**, 766 (1992).

15. T. M. Wolf, G. N. Taylor, T. Venkatesan, and R. R. Kraetsch, *J. Electrochem. Soc.* **131**, 1664 (1984).

16. M. A. Hartney, M. Rothschild, R. R. Kunz, D. J. Ehrlich, and D. C. Shaver, *J. Vac. Sci. Technol. B* **8,** 1476 (1990).

17. R. R. Kunz, M. W. Horn, P. A. Bianconi, D. A. Smith, and J. R. Eschelman, *J. Vac. Sci. Technol. B* **10**, 2554 (1992).

18. M. W. Horn, S. W. Pang, and M. Rothschild, *J. Vac. Sci. Technol. B* **8**, 1493 (1990).

19. M. W. Horn, B. E. Maxwell, R. R. Kunz, M. S. Hibbs, L. M. Eriksen, S. C. Palmateer, and A. R. Forte, *SPIE Proc.* **2438**, 760 (1995).

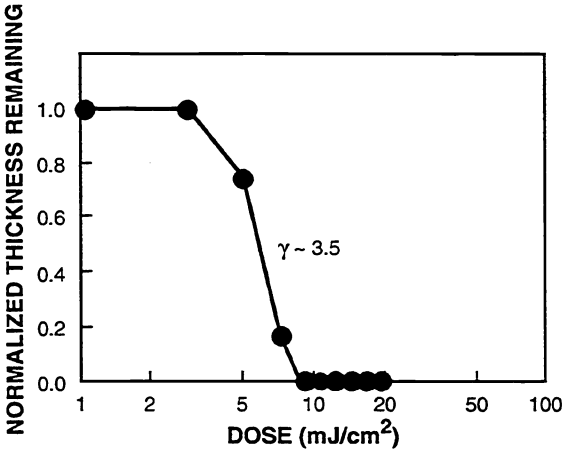

Figure 1 Contrast curve for poly(MMA-*co*-tBMA-*co*-MAA) with 1% bis(*t*-butylphenyl) iodonium triflate, developed in 0.01-N TMAH after a 130°C, 1-minute post-exposure bake.

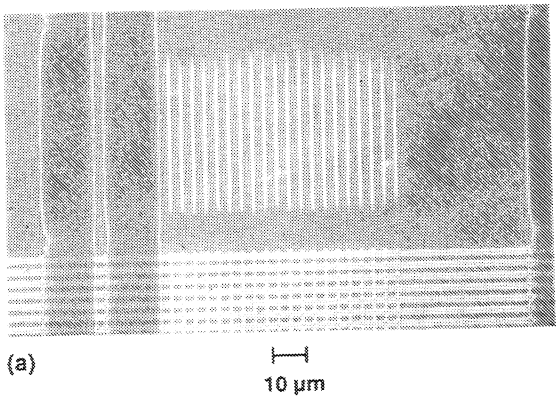

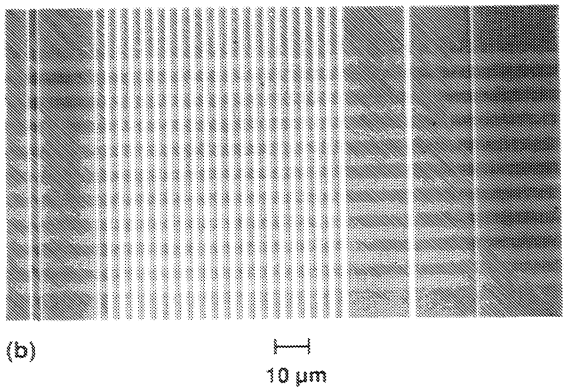

Figure 2 SEMs of resist images over 0.5-µm topography (a) with no ARL, and (b) with 200 nm of 193-ARL. The feature sizes are nominally 2 µm. Note: Transfer of the resist pattern through the ARL was not performed.

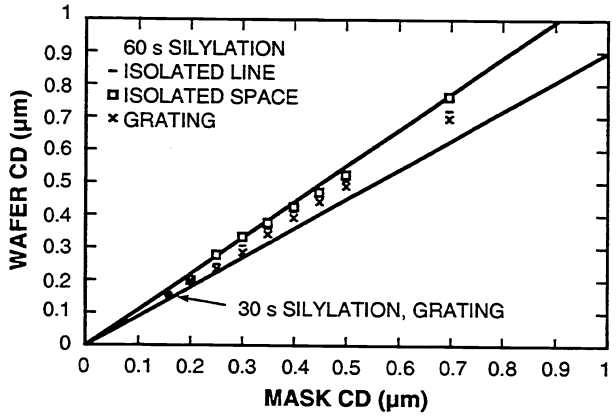

Figure 3 Silylation process linearity at best dose. A 0.76-μm-thick oily(vinylphenol) PVP resist was silylated with dimethylsilyl dimethylamine (DMSDMA) for 60 s, and then was etched under optimized conditions with a 100% overetch. The grating linearity is extended to 0.175 μm for a 30-s silylation time and 25% overetch. The two solid lines are the acceptable performance, i.e., ±10% deviations from the nominal feature size.

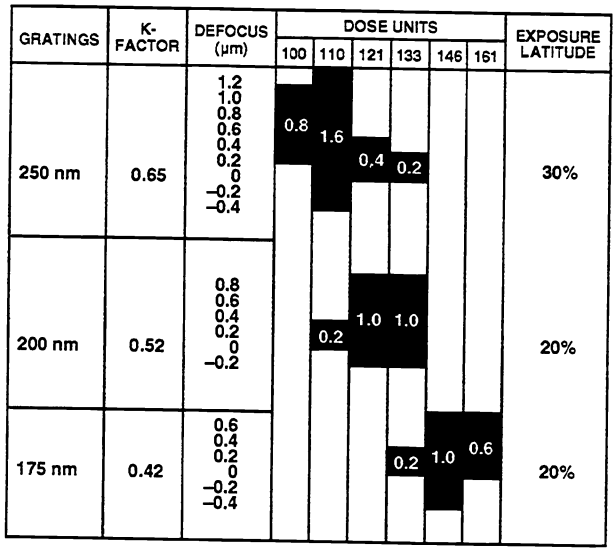

Figure 4 Experimental exposure-dose matrix for 0.25-, 0.20-, and 0.175-μm gratings (±10% CD). Each 193-nm dose unit corresponds to ~1 mJ/cm^2. A 0.50-μm-thick PVP resist was silylated with DMSDMA and then was etched under optimized conditions with a 25% overetch.

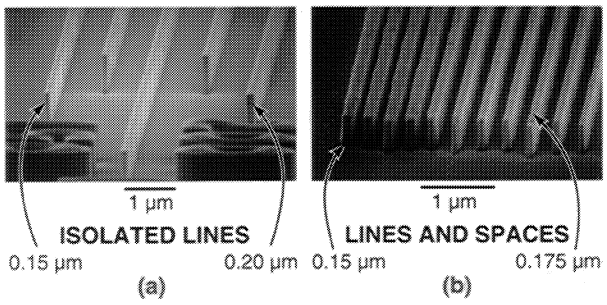

Figure 5 SEMs of 0.15-μm and 0.175 μm (a) isolated and (b) dense features printed with 193-nm top surface imaging. The doses in (a) and (b) were not the same.